Received: 12 March 2021 | Revised: 28 May 2021 | Accepted: 19 June 2021

DOI: 10.1111/cas.15043

ORIGINAL ARTICLE

Cancer Science WILEY

Upregulation of *HOXC9* generates interferon-gamma resistance in gastric cancer by inhibiting the DAPK1/RIG1/STAT1 axis

Yuanxin Tang[1] | Taifang Wang[2] | Yue Yu[2] | Yuhao Yan[1] | Chunli Wu[2]

[1]Department of General Surgery, The Fourth Affiliated Hospital of China Medical University, Shenyang, China

[2]Department of Radiation Oncology, The Fourth Affiliated Hospital of China Medical University, Shenyang, China

Correspondence
Chunli Wu, Department of Radiation Oncology, The Fourth Affiliated Hospital of China Medical University, Shenyang, China.
Email: clwu@cmu.edu.cn

Funding information
Shenyang City, Grant/Award Number: RC200554.

Abstract

Clinical reports indicate that gastric cancer (GC) has a high mortality rate, but its pathological mechanism remains poorly understood. This work integrated bioinformatics analysis with experimental verification to explore novel biomarkers of gastric cancer. First, weighted gene coexpression network analysis was applied to screen significant genes correlated with GC development. Gene set enrichment analysis was also used to unearth the most relevant biological functions of significant genes. As a result, we discovered homeobox C9 (*HOXC9*) as a novel oncogene in GC, primarily through negatively regulating immune response. High expression of *HOXC9* predicted a poor prognosis in GC patients, and knocking down *HOXC9* efficiently enhanced the interferon-gamma (IFNγ)-dependent apoptosis in two GC cell lines as well as organoids from patients. Furthermore, cleaved caspase-3/7 and phosphorylated signal transducer and activator of transcription 1 (p-STAT1) were also significantly enhanced in *HOXC9* knockdown cells and organoids treated with IFNγ. Mechanistically, we found that *HOXC9* inhibited the death-associated protein kinase 1 (*DAPK1*) and its downstream retinoic acid-inducible gene-I (*RIG1*) to generate GC IFNγ resistance. In summary, we identified and confirmed that *HOXC9* generates IFNγ resistance in GC by inhibiting the *DAPK1/RIG1/p-STAT1* axis.

KEYWORDS

DAPK1/RIG1/p-STAT1, gastric cancer, *HOXC9*, IFNγ resistance, weighted coexpression network

1 | INTRODUCTION

Gastric cancer is the second leading cause of cancer death worldwide.[1] Several risk factors for GC development have been reported, including *Helicobacter pylori* infection, gastroesophageal reflux disease, and Barrett's esophagus.[1,2] Gastric cancer has a grave prognosis and the reason mainly lies in the difficulty of early diagnosis.[3] Although many genes and pathways are implicated in the progression of gastric cancer, the mechanism remains largely unknown.[4,5]

Abbreviations: Cor.weighted, weight correlation; Cor.standard, standard correlation; DAPK1, death-associated protein kinase 1; DEG, differentially expressed gene; FDR, false discovery rate; FP, first progression; GC, gastric cancer; GEO, Gene Expression Omnibus; GSEA, Gene Set Enrichment Analysis; HOM, human organoids medium; HOXC9, homeobox C9; ICI, immune checkpoint inhibitor; IFN, interferon; IL, interleukin; IP, immunoprecipitation; OS, overall survival; PD-1, programmed cell death-1; PDO, patient-derived organoid; PPS, post-progression survival; p-STAT1, phosphorylated STAT1; RIG1, retinoic acid-inducible gene-I; ROC, receiver operating characteristic; ssGSEA, single-sample Gene Set Enrichment Analysis; STAT, signal transducer and activator of transcription; TBST, TBS-Tween-20; TCGA, The Cancer Genome Atlas; WGCNA, weighted gene coexpression network analysis.

In past decades, high-throughput microarrays were widely used to identify significant genes correlated with GC development. Li et al found *COL1A1* and *COL1A2* as potential GC prognostic biomarkers of GC by screening of DEGs.[6] Ten core genes in GC tissues were also identified from four original gene chip profiles using DEG screening.[7] Nonetheless, these studies only focused on DEGs and ignored the internal correlation. As such, a biology-related algorithm, WGCNA, was adopted to screen the significant genes correlated with clinical information in cancer and noncancer research by reanalyzing expression profiling data. For instance, Chen et al applied this algorithm and found that *CDH11* was highly correlated with prognosis and progression of GC.[4] Nevertheless, most of these studies lacked basic experimental validation.

Interferon-gamma is proved to exert antitumor efficiency by enhancing T cell-related functions.[8] Mechanistically, IFNγ activates the JAK-STAT signaling cascade by binding with type II IFN receptor.[9] Subsequently, the expression of IFN-induced genes mediates cell cycle arrest and apoptosis.[9] However, not all GC patients respond well to IFNγ and the underlying mechanisms of IFNγ resistance remains largely unknown. Here, the WGCNA algorithm was used to identify hub genes significantly correlated with GC development. Eventually, *HOXC9* was identified as an oncogene in GC. Furthermore, we predicted and experimentally confirmed that *HOXC9* generates IFNγ resistance in GC by inhibiting the *DAPK1/RIG1/p-STAT1* axis.

2 | MATERIALS AND METHODS

2.1 | Gastric cancer data study

The expression profiles of GC were obtained from TCGA and GEO databases. The WGCNA was running on a TCGA-GC cohort, which comprised 33 adjacent normal samples and 375 GC samples. The GSE13911, GSE54129, GSE66229, and GSE34942 datasets were used to validate our findings. GSE13911 included 38 GC samples and 31 normal samples.[10] The GSE54129 dataset included 111 GC and 21 normal samples. Also, the GSE66229 dataset also included 300 GC and 100 normal samples.[11] The GSE34942 dataset contained 56 GC with Lauren subtypes (diffuse or intestinal) and three subtypes (metabolic, proliferative, or invasive).[12]

2.2 | Expression profile preprocessing

First, the distance of each TCGA-GC sample was evaluated by clustering in Pearson's correlation matrices (Figure S1) where no sample outlier was found. Second, the probes of the significant gene were annotated based on the corresponding platform. Finally, DEGs were screened through the "limma" R package under the cut-off of |log2-fold change| >5 and an FDR <0.05.[13]

2.3 | Construction of WGCNA

The "WGCNA" R package was used to construct a network as previously described.[14,15] All screened DEGs were used to calculate the Pearson's correlation, and then a weighted adjacency matrix was constructed through a power function $a_{mn} = |cmn|^{\beta}$, where c_{mn} represents Pearson's correlation between gene m and gene n, and a_{mn} represents adjacency between gene m and gene n. To stress the correlations between genes and penalize weak correlations, a soft threshold β was calculated to construct a scale-free network (Figure 1). Subsequently, a topological overlap matrix was constructed by transforming the adjacency to measure the network connectivity and adjacency. Finally, genes with similar expression profiling were classified into different gene modules by average linkage hierarchical clustering based on the gene dendrogram.

2.4 | Significant module and hub gene selection

To select a significant gene module highly associated with GC progression, the module significance and module eigengenes were calculated based on previously reported studies.[16] Among the significant module, the gene with the highest connectivity, defined as Pearson's correlation (cor.standard) > |0.95| and module membership (cor.weighted) > |0.60|, was considered as the hub gene.

Datasets mentioned above were used to validate the role of the hub gene in GC. The "pROC" package was used to plot the ROC curve.[17] If the area under the curve was greater than 0.7, the candidate genes were considered to be able to distinguish the normal and GC samples. The Kaplan-Meier plotter database (http://kmplot.com/analysis) was used to analyze the prognostic role of *HOXC9* expression in GC. The Oncomine database (https://www.oncomine.org) was used to validate the hub gene expression in GC. The enrichment levels of the 29 immune gene sets and 28 types of immune cells in each GC sample were calculated by the ssGSEA algorithm (Tables S1, S2).[18-20] The "estimate" R package was used to calculate the fraction of stromal, immune, estimate scores, and tumor purity of each sample.[21] The heatmap was constructed using the "pheatmap" package. The relationship between *HOXC9* expression and clinical phenotype was analyzed based on the MEXPRESS database.[22] The correlation between *HOXC9* and *DAPK1/RIG1* was studied in the R2 database (http://r2.amc.nl) (Tumor-Gastric-u133p2-fRMA-192-Tangse15459). Gene Set Enrichment Analysis was used to explore the molecular mechanisms between low and high expression groups according to the hub gene expression under the cut-off criteria of FDR < 0.05, nominal *P* value < 0.05, and |enrichment score| > 0.5.

2.5 | Cells and reagents

Human GC cell lines SGC7901 and MKN45 were purchased from BioVector. These cell lines were maintained in RPMI-1640 (Thermo Fisher Scientific), with 1% GlutaMAX (Thermo Fisher Scientific), 1%

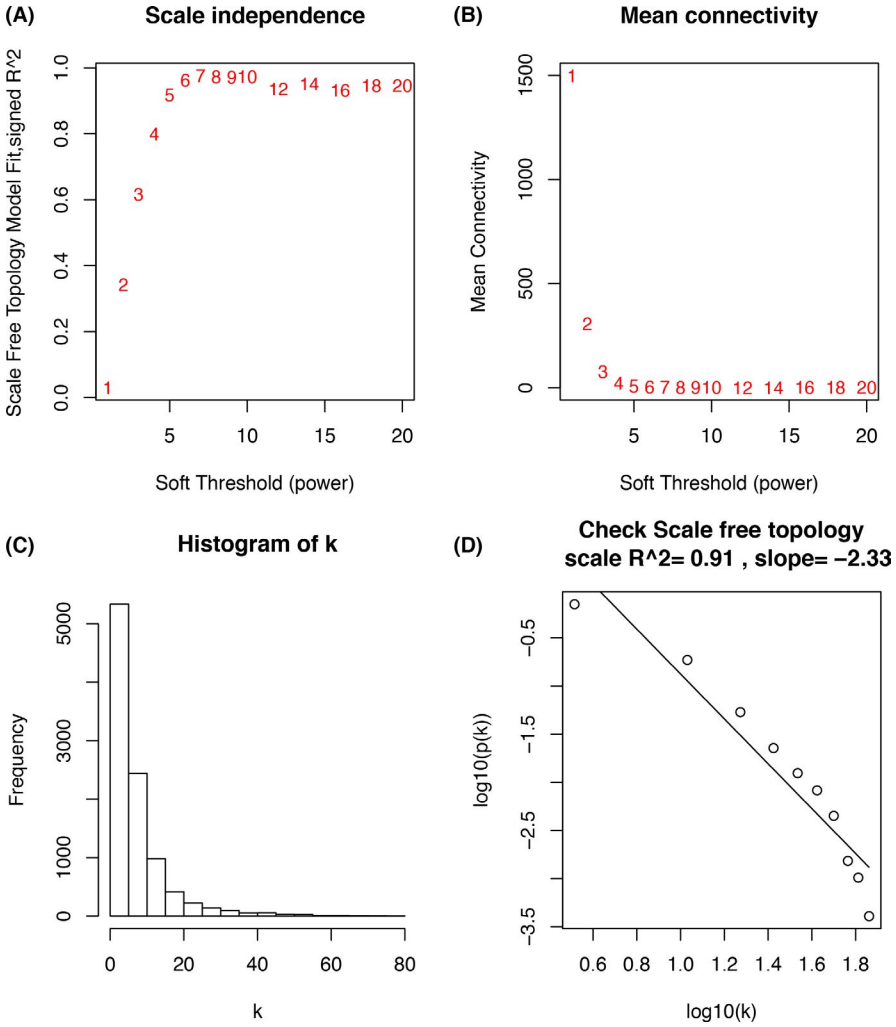

FIGURE 1 Determination of soft-thresholding power in the coexpression network. A, The scale-free fit index was analyzed for various soft-thresholding powers (β). B, Analysis of the mean connectivity for various soft-thresholding powers. C, Histogram of connectivity distribution when β = 5. D, Checking the scale-free topology when β = 5

MEM nonessential amino acid (Thermo Fisher Scientific), and 10% FBS (Hyclone). The cells were grown in a monolayer under standard culture conditions, 5% CO_2 in a 37°C incubator. Cell identity was confirmed by short tandem repeat typing and tested for mycoplasma by PCR.

2.6 | Patients and ethics

A total of 20 GC tissues were collected from patients hospitalized at the Fourth Affiliated Hospital of China Medical University. None of the patients received radiotherapy or chemotherapy before surgery. Ethical approval was obtained from the Fourth Affiliated Hospital of China Medical University. All patients signed an informed consent form.

2.7 | Western blot analysis

MKN45 and SGC7901 cell lysate was transferred into a Triton-based lysis buffer (25 mM HEPES, 0.1 M NaCl, and 1% Triton X-100) containing protease inhibitors (Beyotime). Protein samples (20 μg) were then loaded and separated using SDS-PAGE on 8%-12% Tris-glycine gels before being transferred onto PVDF membranes at 0.2 A for 120 minutes. Following this, the membranes were blocked with western blocking buffer (Beyotime) for 2 hours at 37°C. Subsequently, the membranes were immunoblotted at 4°C overnight using anti-*RIG1* (1:1000 dilution; CST), anti-β-actin (1:2000 dilution; CST), anti-*DAPK1* (1:2000 dilution; CST), anti-*p-STAT1* (1:2000 dilution; CST), anti-*STAT1* (1:2000 dilution; CST). After washing four times with TBST, the membranes were incubated with the HRP-coupled Abs (1:3000 dilution; CST) for 90 minutes. The membranes were washed four times with TBST again and visualized by enhanced chemiluminescence according to the manufacturer's protocol (ECL kit; Beyotime).

For protein IP, SGC7901 cells were lysed with IP buffer (Beyotime) by incubating for 30 minutes at 4°C. Coimmunoprecipitation was carried out with whole-cell lysates using co-IP buffer. Either nuclear or whole-cell lysates were incubated overnight with *STAT1* Abs (1:100 dilution; CST) then for 1 hour with appropriate Dynabeads the following day. Bound proteins were eluted with co-IP buffer for 10 minutes at 100°C before SDS-PAGE analysis.

2.8 | Chromatin IP PCR

For ChIP, cells were fixed with 1% formaldehyde at room temperature for 5 minutes to establish DNA-protein cross-links. Glycine (125 mM) was added to stop the cross-linking and incubated at room temperature for 10 minutes. Cells were washed three times with cold PBS for 5 minutes. One milliliter of cell lysis containing protease inhibitors (MCE) was added to suspend cells and then cell lysates were sonicated using the EpiSonic sonication system to obtain 200-400 bp of chromatin fragments. Chromatin immunoprecipitation was undertaken using the ChIP Assay Kit (P2078; Beyotime). The purified DNA was extracted using a DNA purification kit (Tiangen) and then subjected to quantitative PCR for *DAPK1* promoter detection.

2.9 | Dual luciferase reporter assay

Dual luciferase reporter assays were carried out in a Modulus II Microplate Multimode Reader (Turner Biosystems). A Dual-Lumi Luciferase Assay System was used following the manufacturer's instructions (Beyotime). Briefly, Dual-Lumi luciferase substrate was added to each well. After 15 minutes of incubation, the firefly luminescence signal (FiLuc) was recorded using a plate reader. Then the stop substrate we added for a second incubation of 10 minutes, and the *Renilla* luciferase signal (Relina-Luc) was recorded. Finally, the results were analyzed by calculating the ratio of luminescence from the experimental reporter to the luminescence from the control reporter and normalized to control wells.

2.10 | Immunofluorescence staining

Derived organoids from patients were fixed in 4% paraformaldehyde for 96 hours and were sliced into 5-μm-thick sections. After being deparaffinized and rehydrated in alcohol and water, antigen retrieval was carried out in sodium citrate buffer at 100°C for 5 minutes. Hydrogen peroxide (0.3%) was used to block peroxidase. Sections were incubated with primary Abs, including anti-*HOXC9* (1:200; Abcam), anti-*DAPK1* (1:200 dilution; CST), and anti-*RIG1* (1:200 dilution; CST), at 4°C overnight. After washing with PBST for 15 minutes, samples were incubated with goat anti-rabbit or mouse secondary Ab (1:3000 dilution; CST) and nuclei were stained with DAPI (Beyotime). Images were obtained under a laser scanning confocal microscope (Nikon).

2.11 | Organoid culture

The isolated GC tissue segments were washed three times with cold PBS for 5 minutes and cut open longitudinally. After washing the PBS, the segment was cut into 2-mm pieces. The pieces were digested with collagenase (1 mg/mL collagenase; Sigma Aldrich) in Adv DMEM/F-12 (12634028; Thermo Fisher Scientific) with ROCK inhibitor (Y-27632; 10 μM) for 2 hours at 37°C, followed by collection of the supernatant through a 70-μm filter, which was repeated three times. Patient-derived organoids were cultured in HOM. The composition of HOM included advanced DMEM with 20% R-spondin conditioned medium, 10% Noggin conditioned medium, 1 × B27 (Thermo Fisher Scientific), 1,25 mM N-acetyl cysteine (Selleck Sciences), 10 mM nicotinamide (Selleck Sciences), 50 ng/mL human epidermal growth factor (Selleck Sciences), 500 nM A83-01 (Selleck Sciences), and 10 μM ROCK inhibitor (Selleck Sciences). Derived organoids from patients were fixed in 4% paraformaldehyde for 96 hours and sliced into 5-μm-thick sections. After being deparaffinized and rehydrated in alcohol and water, the sections were subject to conventional H&E staining. The images were observed under a microscope (Olympus, IX83) to determine the pathological changes of the brain tissues.

2.12 | Overexpression and stable KO construction

To establish *HOXC9*-, *DAPK1*-, or *RIG1*-overexpressing cells, SGC7901 and MKN45 cells were transfected with Lipofectamine3000 reagent (Invitrogen). The pCMV-*HOXC9*, pCMV-*DAPK1*, and pCMV-*RIG1* vectors were purchased from Sinobiological. Cells were selected with 500 μg/mL G418 (Beyotime) and KO efficiency was determined by western blot analysis.

To establish *HOXC9*, *DAPK1*, or *RIG1* knockdown cells, SGC7901 and MKN45 cells were transfected with Lipofectamine3000 reagent (Invitrogen) and siRNA. The siRNAs were purchased from Tsingke. The siRNA sequences were as follows: *HOXC9* si-1, 5′-CGTGCCCTCTCAGTCGTCCGTGGTA-3′; *HOXC9* si-2, 5′-CCGTCGGTATGAGGTGGCCCGGGTT-3′; *DAPK1* si-1, 5′-GGGTGCCACCGTTGCCGCAGGCTGG–3′; DAPK1 si-2, 5′-CCGTTGCCGCAGGCTGGAGAGAGAT-3′; *RIG1* si-1, 5′-TGCTTATATGTGAACATCATCTTAA -3′; and RIG1 si-2, 5′-CCACAGATTCTTGTGAACAACCTTA-3′.

To establish *HOXC9* knockdown cells, SGC7901 and MKN45 cells were transfected with Lipofectamine3000 reagent (Invitrogen). The PLKO.1-Puro vectors were purchased from GenePharma. The shRNA sequences were as follows: *HOXC9* Sh1, 5′-CCGGCCGCAGCTACCCGGACTACATCTCGAGATGTAGTCCGGGTAGCTGCGGTTTTT-3′; *HOXC9* Sh2, 5′-CCGGCCGGGTTCTCAATCTCACCGACTCGAGTCGGTGAGATTGAGAACCCGGTTTTT-3′; and ShCtrl, 5′-GGAATCTCATTCGATGCATAC-3′.

2.13 | Cell viability assay

Cell viability was analyzed using CCK-8 assays. Gastric cancer cells were seeded at 10 000 cells per well in a 96-well plate, and CCK-8 solution was added in the wells and incubated at 37°C for 2 hours. The absorbance value (optical density) was measured at 490 nm

using a microplate reader (ELx800; BioTek). Each experiment was repeated at least three times.

2.14 | Prediction of ICI treatment response

We used the TIGER database (http://tiger.canceromics.org/#/home) to show the *HOXC9* expression between responders and nonresponders in several melanoma ICI-treated cohorts (N ≥ 10). In addition, to predict the correlation between *HOXC9* and ICI treatment in GC, we applied the SubMap analysis (Gene Pattern). This bioinformatics method helped identify genetic similarity in gene expression profiles between subgroups from different independent cohorts.[23] Thus, we used this algorithm to measure the similarity of *HOXC9*-high and *HOXC9*-low groups with different groups of patients from one melanoma ICI cohort.[24]

2.15 | Statistical analysis

In this study, statistical analyses were undertaken using R 3.6.1 software and GraphPad Prism 7.0. Data were expressed as the means ± SEM. Comparisons between two groups were carried out by unpaired Student's *t* test or one-way ANOVA. Correlations between groups were determined by Pearson's correlation test. Survival rates were analyzed by the Kaplan-Meier method. The sample number (n) indicates the number of independent biological samples in each experiment. Generally, all experiments were carried out with n ≥ 3 biological replicates. $P < .05$ was considered statistically significant.

3 | RESULTS

3.1 | Red module as the significant module and *HOXC9* as the hub gene

A total of 9376 DEGs were run for the WGCNA analysis and the soft threshold was calculated as 5 for scale-free network construction (Figure 1). As shown in Figure 2A, all DEGs were divided into 11 gene modules (Figure 2A). Among these modules, the red module showed both the highest module significance and module eigengene (Figure 2B,C). Therefore, genes in the red module were selected for further screening of hub genes. *HOXC9* was selected as the hub gene because of the highest cor.weighted and cor.standard (excluding the first noncoding RNA). Table 1 shows the genes based on both weighted and standard correlation coefficients. Collectively, our data predicted *HOXC9* as the most significant gene associated with GC progression.

3.2 | Upregulation of *HOXC9* in GC

In the test databases of GEO and Oncomine, *HOXC9* expression was significantly upregulated in GC samples compared to that in adjacent normal samples (Figure 3A,B). The ROC analysis indicated that *HOXC9* expression effectively distinguished GC from normal gastric tissues based on the TCGA database (Figure 3C). Furthermore, in the test set of GSE34942, *HOXC9* expression was significantly upregulated in the proliferative subtype compared to the metabolic and invasive subtypes, whereas there were no

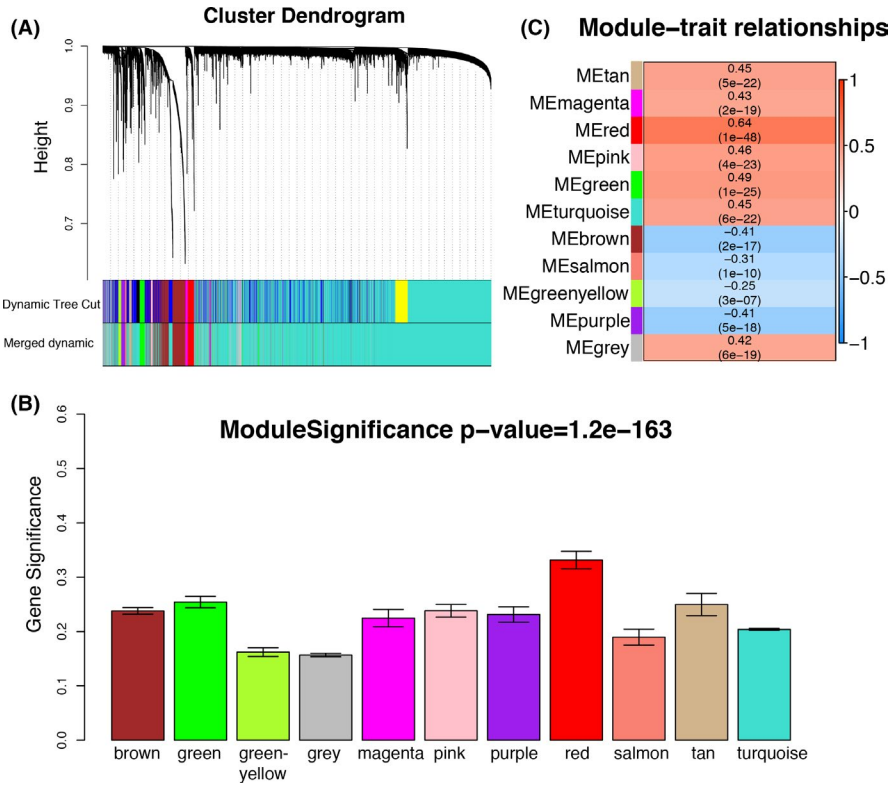

FIGURE 2 Red module as the most significant module associated with gastric cancer (GC) progression. A, All differentially expressed genes clustered based on a dissimilarity measure (1 − topological overlap matrix) and shown on a dendrogram. B, Distribution of average gene significance and errors in all the modules highly associated with GC. C, Correlation heatmap between module eigengenes (ME) and GC progression

TABLE 1 Hub genes in the red module ranked by weighted correlation (Cor.) and standard correlation

Genes	Ensembl_ID	Cor.weighted	Cor.standard	FDR	LogFC
RP11-181E10.3	ENSG00000271590	0.970894525	0.672316376	5.33E-30	6.486526
HOXC9	ENSG00000180806	0.950078602	0.664253817	1.92E-29	8.650675
ESM1	ENSG00000164283	0.954652276	0.632806716	1.36E-30	4.758556

Abbreviations: FC, fold change; FDR, false discovery rate.

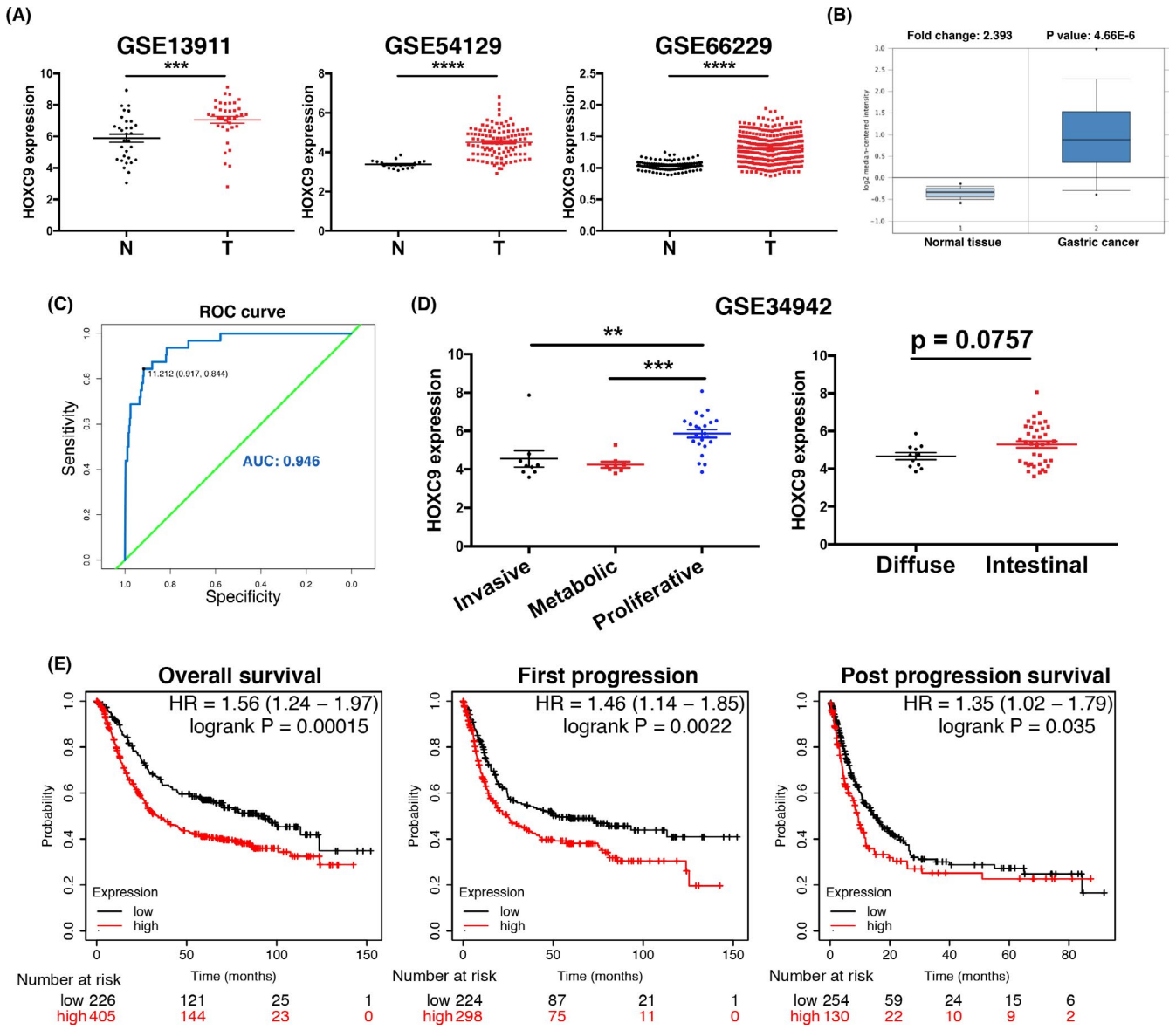

FIGURE 3 *HOXC9* is upregulated in gastric cancer (GC) and serves as an indicator of poor prognosis. A, Comparison of *HOXC9* expression between normal tissues (N) and GC samples (T) based on the GSE13911, GSE54129, and GSE66229 datasets. B, Comparison of *HOXC9* expression between normal tissues and GC samples based on the Oncomine database. C, The receiver operating characteristic (ROC) curve shows the diagnostic efficiency of *HOXC9* based on The Cancer Genome Atlas GC cohort (normal tissues vs gastric cancer samples). AUC, area under the ROC curve. D, Comparison of *HOXC9* expression in metabolic, proliferative, or invasive subtypes (left) and Lauren subtypes (diffuse or intestinal) (right) of GC based on the GSE34942 dataset. E, Survival analysis of *HOXC9* based on the kmplot database. $^{**}P < .01$, $^{***}P < .001$, $^{****}P < .0001$

significant difference between diffuse and intestinal subtypes (Figure 3D). The survival analysis found that high *HOXC9* expression showed a poor prognosis of OS, FP, and PPS in GC patients (Figure 3E). Nevertheless, *HOXC9* expression was not associated with clinical phenotype based on the public MEXPRESS database (Figure S2).

3.3 | Negative regulation of immune response in GC by *HOXC9*

To identify potential biological functions of *HOXC9*, GSEA was applied. Eight gene sets associated with inflammatory response were finally enriched, including "allograft rejection," "inflammatory response," "interferon gamma response," "IL2 STAT5 signaling," "IL6 JAK STAT3 signaling," "TNFA signaling via NFKB," "UV response DN," and "epithelial mesenchymal transition" (Figure 4A). Moreover, we applied several published immune-related tools to decipher the immune heterogeneity between *HOXC9*-high and *HOXC9*-low expression groups. First, we computed the stromal and immune score of each group by the "estimate" R package. The results showed that lower levels of stromal, immune, and estimate scores were found in the *HOXC9*-high expression group (Figure 4B). A reduction of tumor purity was also observed in the *HOXC9*-high group (Figure 4B), indicating that this group might contain low levels of immune cells. It was found that higher *HOXC9* showed a high negative correlation with these scores (Figure 4C). The ssGSEA algorithm further confirmed that patients in the *HOXC9*-high expression group showed lower fractions of 29 immune-related functions (Figure S3). These data indicated that high *HOXC9* expression could promote the formation of cold tumor microenvironment.

To clarify the relationship between the high expression of *HOXC9* and the formation of cold tumors, we analyzed 28 immune cells in the tumor microenvironment. The heatmap showed that almost all immune cells had significantly reduced infiltration in the *HOXC9*-high expression group (Figure 4D). Furthermore, the "limma" analysis results showed that, among the immune cells with significantly reduced infiltration in the *HOXC9*-high expression group, the top seven with the most significant fold change were mainly T cells, including Type 1 T helper, central memory CD8 T, effector memory CD4 T, natural killer, and effector memory CD8 T cells (Figure 4E). Therefore, these data indicated that high *HOXC9* expression could form cold tumors by inhibiting the activation of T cells.

3.4 | Knockdown of *HOXC9* expression increased IFNγ-dependent apoptosis

To further evaluate the role of *HOXC9* in GC, the *HOXC9* expression in SGC7901 and MKN45 cells was silenced by siRNA (Figure 5A). Consequently, knockdown of *HOXC9* effectively enhanced IFNγ-dependent apoptosis (Figure 5B,C). However, overexpression of *HOXC9* impaired IFNγ-dependent apoptosis (Figure S4A), indicating that *HOXC9* acted as the downstream molecule of IFNγ to induce GC cells apoptosis. To further demonstrate our data in vivo, we established PDOs. Intriguingly, we found that GC tissues with high *HOXC9* levels had IFNγ resistance (Figure 5D-F). More importantly, a high correlation was observed between *HOXC9* level and IFNγ-induced apoptosis (Figure 5G), corroborating the findings in the cell line. As a member of the STAT family, STAT1 is an essential component of IFN signaling that mediates several cellular functions in response to CD8 T cells. Here, upregulation of p-STAT1 and cleaved caspase-3/7 were observed in *HOXC9* KO cell lines (Figure 5H). Consistently, overexpression of *HOXC9* impaired the IFNγ-dependent upregulation of p-STAT1 and cleaved caspase-3/7 (Figure S4B). Similar outcomes were observed in PDOs (Figure 5I). More importantly, a high negative correlation was observed between *HOXC9* and p-STAT1 levels (Figure 5J). Collectively, these findings indicate that *HOXC9* negatively regulates the IFNγ signaling pathway in GC cells and PDOs, inducing resistance of GC cells to IFNγ.

3.5 | *HOXC9* induced IFNγ resistance by downregulating DAPK1/RIG1 expression

Next, we investigated the molecular pathway through which *HOXC9* repressed cancer immunity in GC. Previous data revealed that *HOXC9* directly inhibited the transcription of DAPK1, and knockdown of DAPK1 attenuated RIG1 expression, a cytosolic pattern recognition receptor that initiates innate antiviral immunity and cancer immunotherapy.[25-27] Consistently, upregulation of DAPK1 and RIG1 were observed in SGC7901 and MKN45 cells transfected with *HOXC9* siRNA (Figure 6A). Moreover, our ChIP and dual-luciferase analyses showed that *HOXC9* was enriched in the promoter sites of DAPK1 and inhibited DAPK1 expression (Figure 6B,C), confirming that *HOXC9* might attenuate DAPK1 activation and negatively regulate RIG-I expression.

Previous studies have reported *RIG1* amplifies IFN-JAK-STAT effector signaling by diminishing the interaction between *SHP1* and *STAT1* in cancer cells.[28] We also confirmed that *RIG1* and *STAT1* interact with each other with or without IFNγ using IP. Moreover, we found that *SHP1* was coimmunoprecipitated with *STAT1*, but this interaction was increased by *RIG1* KO (Figure S4C). ClusPro server was used to estimate protein-protein interaction.[29] We found that there might be interaction domains between *RIG1* and *STAT1* (Figure S4D). Hence, *RIG1* promotes *STAT1* activation mainly through suppressing the interaction and inhibition of *STAT1* by *SHP1* and competitively binding *STAT1*.

To further confirm the role of the *HOXC9-DAPK1-RIG1* axis in IFNγ resistance, we knocked out *DAPK1* or *RIG1* in *HOXC9*-silenced SGC7901 and MKN45 cell lines by siRNA (Figure 6D,E). Consistently, we found that *RIG1* was significantly downregulated in GC cells with knocked out DAPK1 (Figure 6D). Intriguingly, *DAPK1* or *RIG1* KO efficiently reversed the SGC7901 and MKN45 sensitivity to IFNγ induced by silencing *HOXC9* (Figure 6F). Similar results were observed in PDOs (Figure 6G). Importantly, *DAPK1* or *RIG1* KO also efficiently inhibited the expression of *p-STAT1* in SGC7901 and MKN45 cells, induced by IFNγ (Figure 6H,I). Consistently, reconstitution of *HOCX9* in *HOCX9*-silenced cells can downregulate *RIG1* expression. In contrast, the overexpression of *DAPK1* can impair *HOXC9*-mediated *RIG1* downregulation (Figure S4E). To further support the correlation between *HOXC9* and DAPK1/RIG1 in vivo, we analyzed the R2 online database (http://r2.amc.nl) and found that *HOXC9* was

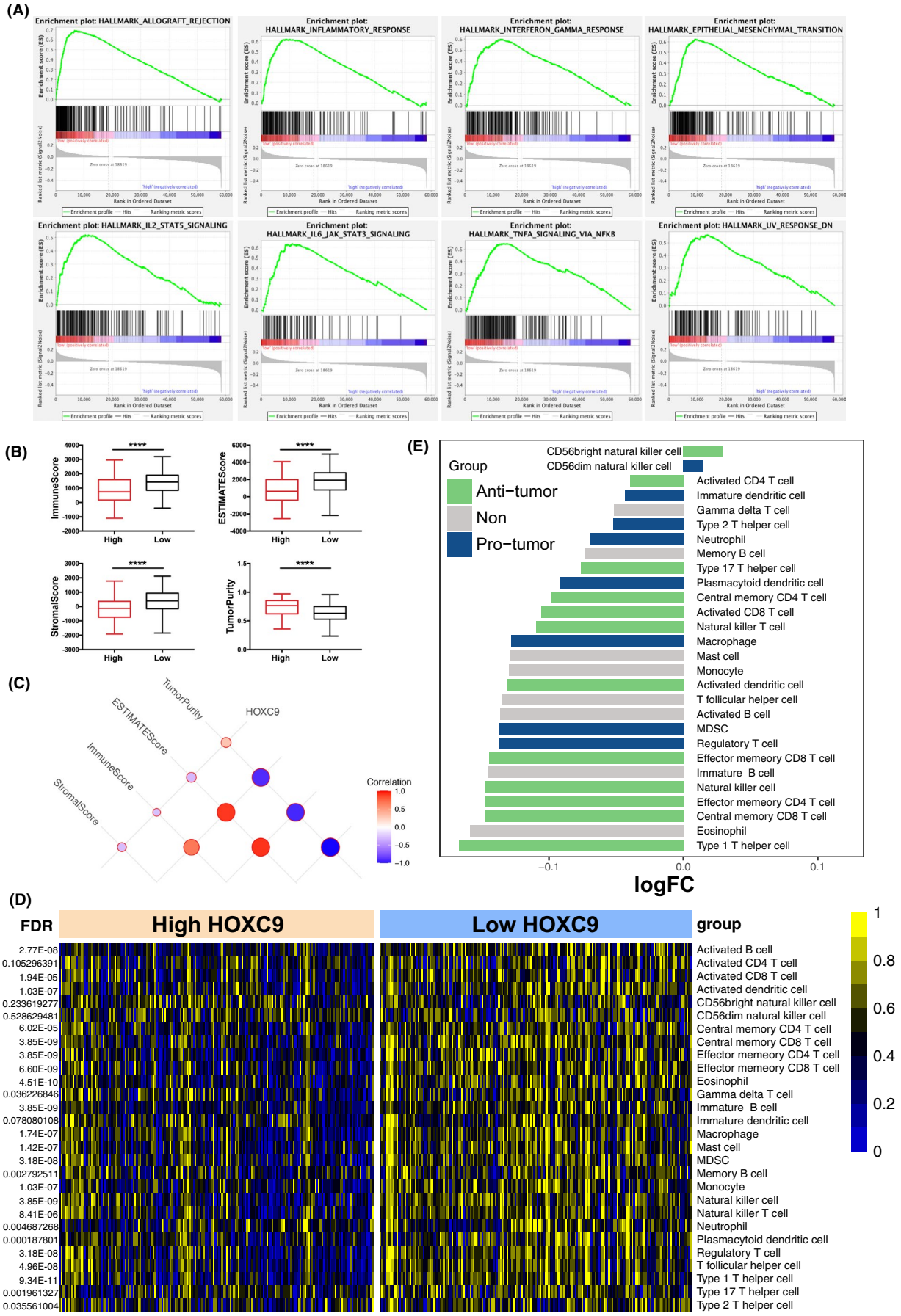
(A)
Enrichment plot: HALLMARK_ALLOGRAFT_REJECTION
Enrichment plot: HALLMARK_INFLAMMATORY_RESPONSE
Enrichment plot: HALLMARK_INTERFERON_GAMMA_RESPONSE
Enrichment plot: HALLMARK_EPITHELIAL_MESENCHYMAL_TRANSITION
Enrichment plot: HALLMARK_IL2_STAT5_SIGNALING
Enrichment plot: HALLMARK_IL6_JAK_STAT3_SIGNALING
Enrichment plot: HALLMARK_TNFA_SIGNALING_VIA_NFKB
Enrichment plot: HALLMARK_UV_RESPONSE_DN
(B)
ImmuneScore
ESTIMATEScore
StromalScore
TumorPurity
High
Low
****
(C)
HOXC9
TumorPurity
ESTIMATEScore
ImmuneScore
StromalScore
Correlation
(E)
Group
Anti−tumor
Non
Pro−tumor
CD56bright natural killer cell
CD56dim natural killer cell
Activated CD4 T cell
Immature dendritic cell
Gamma delta T cell
Type 2 T helper cell
Neutrophil
Memory B cell
Type 17 T helper cell
Plasmacytoid dendritic cell
Central memory CD4 T cell
Activated CD8 T cell
Natural killer T cell
Macrophage
Mast cell
Monocyte
Activated dendritic cell
T follicular helper cell
Activated B cell
MDSC
Regulatory T cell
Effector memeory CD8 T cell
Immature B cell
Natural killer cell
Effector memeory CD4 T cell
Central memory CD8 T cell
Eosinophil
Type 1 T helper cell
logFC
(D)
FDR
High HOXC9
Low HOXC9
group
2.77E-08 Activated B cell
0.105296391 Activated CD4 T cell
1.94E-05 Activated CD8 T cell
1.03E-07 Activated dendritic cell
0.233619277 CD56bright natural killer cell
0.528629481 CD56dim natural killer cell
6.02E-05 Central memory CD4 T cell
3.85E-09 Central memory CD8 T cell
3.85E-09 Effector memeory CD4 T cell
6.60E-09 Effector memeory CD8 T cell
4.51E-10 Eosinophil
0.036226846 Gamma delta T cell
3.85E-09 Immature B cell
0.078080108 Immature dendritic cell
1.74E-07 Macrophage
1.42E-07 Mast cell
3.18E-08 MDSC
0.002792511 Memory B cell
1.03E-07 Monocyte
3.85E-09 Natural killer cell
8.41E-06 Natural killer T cell
0.004687268 Neutrophil
0.000187801 Plasmacytoid dendritic cell
3.18E-08 Regulatory T cell
4.96E-08 T follicular helper cell
9.34E-11 Type 1 T helper cell
0.001961327 Type 17 T helper cell
0.035561004 Type 2 T helper cell

FIGURE 4 High expression of *HOXC9* inhibits immune microenvironment in gastric cancer (GC). A, Gene Set Enrichment Analysis plots of significant gene sets showing positive correlation with higher expression of *HOXC9* in The Cancer Genome Atlas (TCGA) cohort. B, Comparison of ImmuneScore, StromalScore, ESTIMATEScore, and TumorPurity between *HOXC9*-high and *HOXC9*-low expression groups. C, Correlation between *HOXC9* expression and immune scores, stromal scores, estimate score, and tumor purity in the TCGA cohort. D, Heatmap showing the difference in 28 types of immune cells between high- and low-*HOXC9* groups of the TCGA cohort. E, Bar graph showing the |log2-fold change| of the 28 regulated immune cells infiltrating high vs low *HOXC9*-expressing GC samples based on the TCGA cohort. $^{**}P < .01$, $^{***}P < .001$, $^{****}P < .0001$

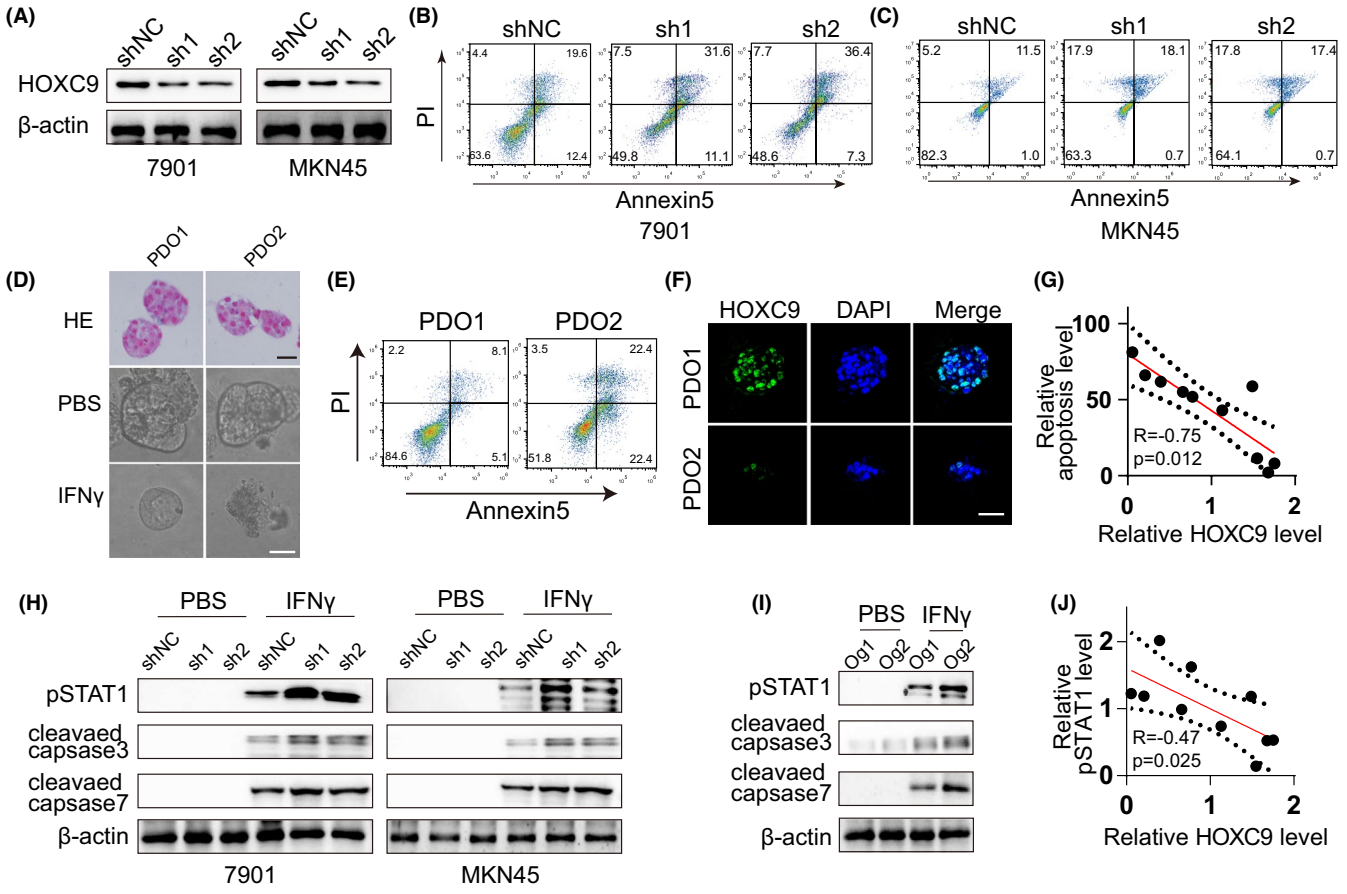

FIGURE 5 Knockdown of *HOXC9* expression increased interferon-gamma (IFNγ)-dependent apoptosis. A, Western blot assay of *HOXC9* expression in SGC7901-shNC, SGC7901-sh1, SGC7901-sh2, MKN45-shNC, MKN45-sh1, and MKN45-sh2 cells. B, After treatment with IFNγ (100 ng/mL) for 48 h, SGC7901-shNC, SGC7901-sh1, and SGC7901-sh2 cells were isolated, stained with annexin V and propidium iodide (PI) and analyzed by flow cytometry for apoptosis detection. C, After treatment with IFNγ (100 ng/mL) for 48 h, MKN45-shNC, MKN45-sh1, and MKN45-sh2 cells were isolated, stained with annexin V and PI, and analyzed by flow cytometry for apoptosis detection. D, H&E staining and cell microscope photographs of patient-derived organoids (PDOs) with *HOXC9*-high and -low expression treated with IFNγ (100 ng/mL) for 48 h. Bar = 25 μm. E, After treating with IFNγ (100 ng/mL) for 48 h, PDOs with *HOXC9*-high and -low expression were isolated, stained with annexin V and PI, and analyzed by flow cytometry for apoptosis detection. F, Confocal images of PDOs with *HOXC9*-high and -low expression. Bar = 25 μm. G, Pearson's correlation of *HOXC9* expression and the apoptosis rate. H, SGC7901-shNC, SGC7901-sh1, SGC7901-sh2, MKN45-shNC, MKN45-sh1, and MKN45-sh2 cells were treated with PBS or IFNγ (100 ng/mL) for 48 h. Cell lysates were collected and phosphorylated STAT1 (p-STAT1), cleavaed-caspase-3, and cleavaed-caspase-7 were analyzed by western blot. β-Actin was used as internal reference. I, PDOs with *HOXC9*-high and -low expression were treated with PBS or IFNγ (100 ng/mL) for 48 h. PDOs were then washed with PBS and cell lysates were collected and p-STAT1, cleavaed-capsase-3, and cleavaed-capsase-7 were analyzed by western blot. β-Actin was used as internal reference. J, Pearson's correlation of *HOXC9* expression and p-STAT1 expression. $^{*}P < .05$, $^{**}P < .01$, $^{***}P < .001$, $^{****}P < .0001$

significant negatively correlated with *DAPK1* ($r = -.242$, $P = 4.14e-04$) and *RIG1* ($r = -.314$, $P = 9.01e-06$), while *DAPK1* was significantly positively correlated with *RIG1* ($r = .328$, $P = 3.49e-06$) (Figure S5). These results suggested that *HOXC9* downregulated the expression of *DAPK1* downstream molecule *RIG1* to induce the development of GC IFNγ resistance.

3.6 | Downregulation of *HOXC9* predicted a promising response to anti-PD-1 therapy

Finally, we explored the correlation between *HOXC9* expression and sensitivity to therapy using ICIs. Based on the TIGER database,

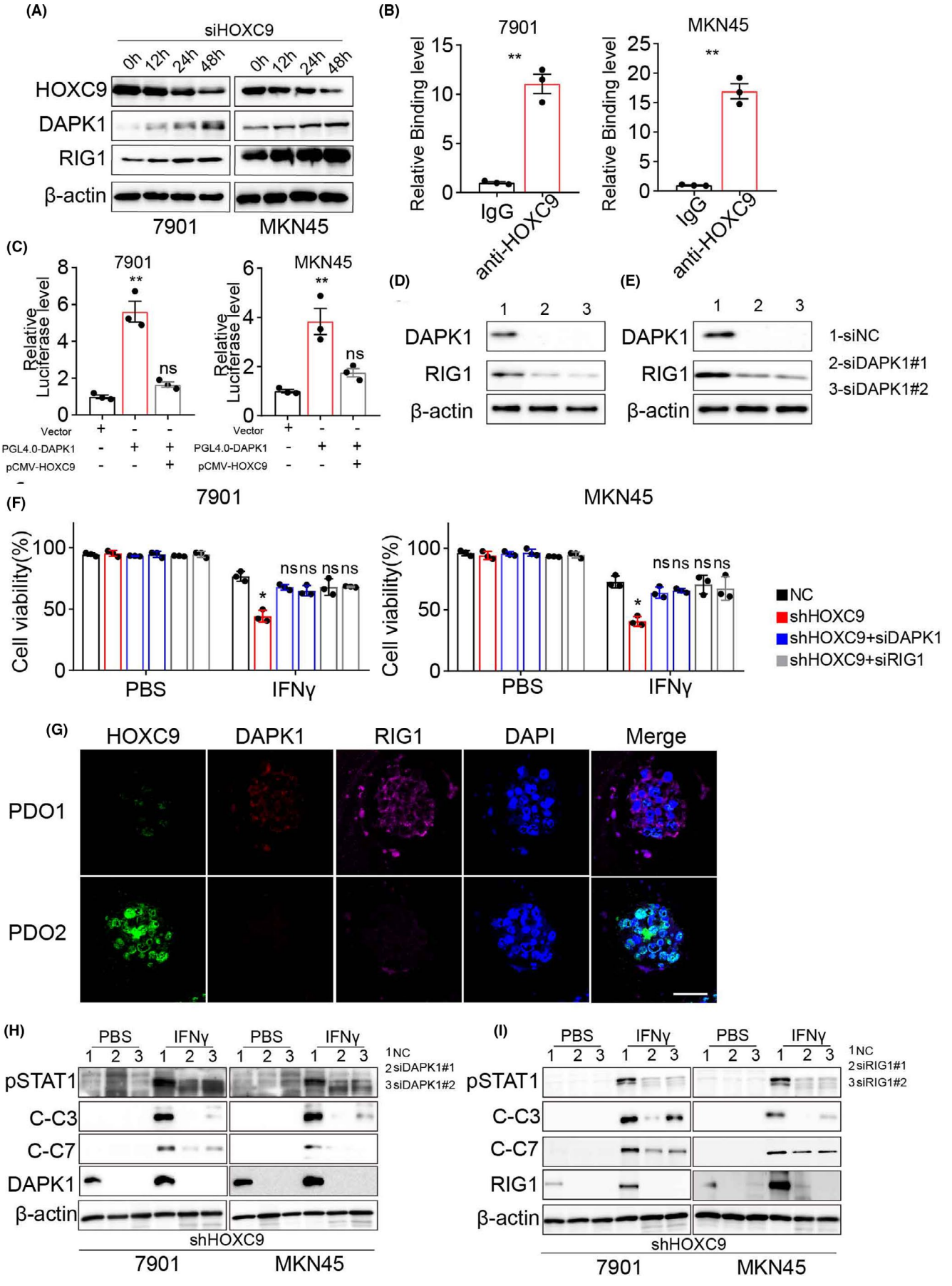
(A)
siHOXC9
0h 12h 24h 48h 0h 12h 24h 48h
HOXC9
DAPK1
RIG1
β-actin
7901
MKN45
(B)
7901
MKN45
Relative Binding level
**
IgG
anti-HOXC9
(C)
7901
MKN45
Relative Luciferase level
**
ns
Vector
PGL4.0-DAPK1
pCMV-HOXC9
(D)
1 2 3
DAPK1
RIG1
β-actin
(E)
1 2 3
DAPK1
RIG1
β-actin
1-siNC
2-siDAPK1#1
3-siDAPK1#2
(F)
7901
MKN45
Cell viability(%)
PBS
IFNγ
ns ns ns ns
*
NC
shHOXC9
shHOXC9+siDAPK1
shHOXC9+siRIG1
(G)
HOXC9
DAPK1
RIG1
DAPI
Merge
PDO1
PDO2
(H)
PBS IFNγ PBS IFNγ
1 2 3 1 2 3 1 2 3 1 2 3
1NC
2siDAPK1#1
3siDAPK1#2
pSTAT1
C-C3
C-C7
DAPK1
β-actin
shHOXC9
7901
MKN45
(I)
PBS IFNγ PBS IFNγ
1 2 3 1 2 3 1 2 3 1 2 3
1NC
2siRIG1#1
3siRIG1#2
pSTAT1
C-C3
C-C7
RIG1
β-actin
shHOXC9
7901
MKN45

FIGURE 6 *HOXC9* induced interferon-gamma (IFNγ) resistance through downregulating *DAPK1/RIG1* expression. A, SGC7901 and MKN45 cells were transfected with *HOXC9* siRNA for different times. Cell lysates were collected and analyzed for *HOXC9*, *DAPK1*, and *RIG1* by western blot. β-Actin was used as internal reference. B, ChIP assay of *HOXC9* binding with *DAPK1* promoter in SGC7901 and MKN45 cells. IgG was used as a negative control. C, SGC7901 and MKN45 cells were transfected with vector, *DAPK1*, and *HOXC9* overexpression plasmids. The dual luciferase assay shows that *HOXC9* activated DAPK1 promoter in SGC7901 and MKN45 cells. D, E, SGC7901 and MKN45 cells were transfected with si-control (siNC) and *DAPK1* siRNA for 48 h. Cell lysates were collected and *DAPK1* and *RIG1* were analyzed by western blot. β-Actin was used as internal reference. F, Cell viability assay of SGC7901 and MKN45 cells transfected with different shRNA plasmids after treatment with PBS or IFNγ (100 ng/mL) for 48 h. G, *HOXC9*, *DAPK1*, and *RIG1* expression of patient-derived organoids (PDOs) with *HOXC9*-high and -low expression. Bar = 25 μm. H, SGC7901-shHOXC9 and MKN45-shHOXC9 cells were transfected with siNC and *DAPK1*-siRNA for 48 h, and then treated with PBS or IFNγ (100 ng/mL) for 48 h. Cell lysates were collected and *DAPK1*, *p-STAT1*, cleaved caspase-3 (*C-C3*), and cleaved caspase-7 (*C-C7*) were analyzed by western blot. β-Actin was used as internal reference. I, SGC7901-shHOXC9 and MKN45-shHOXC9 cells were transfected with siNC and *RIG1*-siRNA for 48 h, and then treated PBS or IFNγ (100 ng/mL) for 48 h. Cell lysates were collected and *RIG1*, *p-STAT1*, *C-C3*, and *C-C7* were analyzed by western blot. β-Actin was used as internal reference. $^{*}P < .05$, $^{**}P < .01$, $^{***}P < .001$, $^{****}P < .0001$

we compared the *HOXC9* expression between responders and nonresponders in several melanoma ICI-treated cohorts (n ≥ 10). In the GSE91061 and phs000452 datasets, we found that the responders showed lower levels of *HOXC9* expression (Figure 7A,B). Furthermore, in the PRJEB23709 dataset, *HOXC9* expression decreased significantly in the responder group, especially when anti-PD-1 was used alone (Figure 7C,D). However, we found that there was no significant difference in *HOXC9* expression when anti-CTLA4 and anti-PD-1 were used in combination (Figure 7E). Interestingly, male patients seem to have a more significant decline in *HOXC9* expression, although there was no statistical difference (Figure 7B,D). To better clarify the relationship between *HOXC9* expression and immunotherapeutic response in GC, we used the SubMap algorithm and found that patients with low *HOXC9* expression could be more sensitive to anti-PD-1 therapy (Bonferroni-corrected $P = .024$). Taken together, our findings indicated that *HOXC9* could be a new biomarker for anti-PD-1 therapy.

4 | DISCUSSION

Through WGCNA, this study identified *HOXC9* as a novel oncogene, which highly correlated with the progression and prognosis of GC. The GSEA results further revealed that *HOXC9* could negatively regulate immune response. Regarding validation, knockdown of *HOXC9* expression effectively enhanced IFNγ-dependent apoptosis in SGC7901 and MKN45 cells and PDOs. Furthermore, cleaved caspase-3/7 and p-STAT1 were significantly enhanced in *HOXC9* knockdown cells and organoids treated with IFNγ. Mechanistically, we found that *HOXC9* inhibited *DAPK1* and the downstream *RIG1* to generate GC IFNγ resistance.

Of note, *HOXC9* belongs to the homeobox transcription factor family, which is implicated in cell cycle, differentiation, migration, and other biological processes.[30] Thus, the dysregulation of *HOXC9* expression is strongly linked to multiple malignant tumor progression, including colorectal cancer,[31] breast cancer,[32] and glioblastoma.[33] Furthermore, Zhao et al first reported significant upregulation of *HOXC9* expression in GC compared to normal tissues.[30] Similarly, based on public databases, our findings confirmed that *HOXC9* was an oncogene in GC. Moreover, we found that patients with higher expression level of *HOXC9* predicted a poor prognosis in terms of OS, FP, and PPS, indicating *HOXC9* was an unfavorable prognosis factor in GC.

Next, we explored the molecular mechanism of *HOXC9* promoting GC progression. Peng et al reported that upregulation of microRNA-26a inhibited metastasis and self-renewal through downregulated *HOXC9*.[34] Based on the GSEA results, this work indicated that *HOXC9* was highly and negatively correlated with immune response. Furthermore, the high *HOXC9* group revealed low levels of immune-related biological functions compared to the low *HOXC9* group. At present, information on the relationship between *HOXC9* and tumor immunity remain unreported. Nonetheless, it was evident that other members of the HOX family modulated inflammatory response in multiple types of cancer.[35] For example, upregulation of *HOXB9* expression induced higher levels of *IL-8* in breast cancer, which was related to tumor development.[36] Also, *HOXA9* inhibited innate immune response by suppressing the nuclear factor-κb (nf-κb) pathway.[37] As such, for the first time, we reported the immunomodulatory mechanism of *HOXC9* in GC.

Accumulating evidence has implicated effective T cell response in patients who temporarily benefit from surgical resection and/or chemotherapy.[38,39] Remarkable response rates for PD-1 or other immunotherapies have been reported in the treatment of GC.[40-43] Unfortunately, not all patients benefit equally from immunotherapy.[44] Primary or acquired immunotherapy resistance is a primary concern, thus, the understanding of resistance mechanisms is critical for advancing GC treatment. Additionally, IFNγ plays a critical role in an antitumor effect through extrinsic or tumor cell-intrinsic mechanisms.[45,46] Concerning the extrinsic antitumor property, IFNγ promotes antitumor immunity and stimulates tumors to infiltrate immune cell recognition and elimination.[45] Regarding the tumor cell-intrinsic mechanism, studies showed that IFNγ exerts a strong antitumor role by promoting growth arrest and cell death through *p-STAT1* signaling.[45] More importantly, resistance to immunotherapy has been attributed to mutated IFNγ signaling, as well as IFNγ resistance protecting from cytokine-induced cell cycle arrest/apoptosis.[47-49] In the present study, we found that the expression of *HOXC9* also induced the IFNγ resistance phenotypes of GC cells in cell lines and PDOs by suppressing phosphorylation of STAT1. We also found that downregulation of *DAPK1* signaling induced by *HOXC9* caused

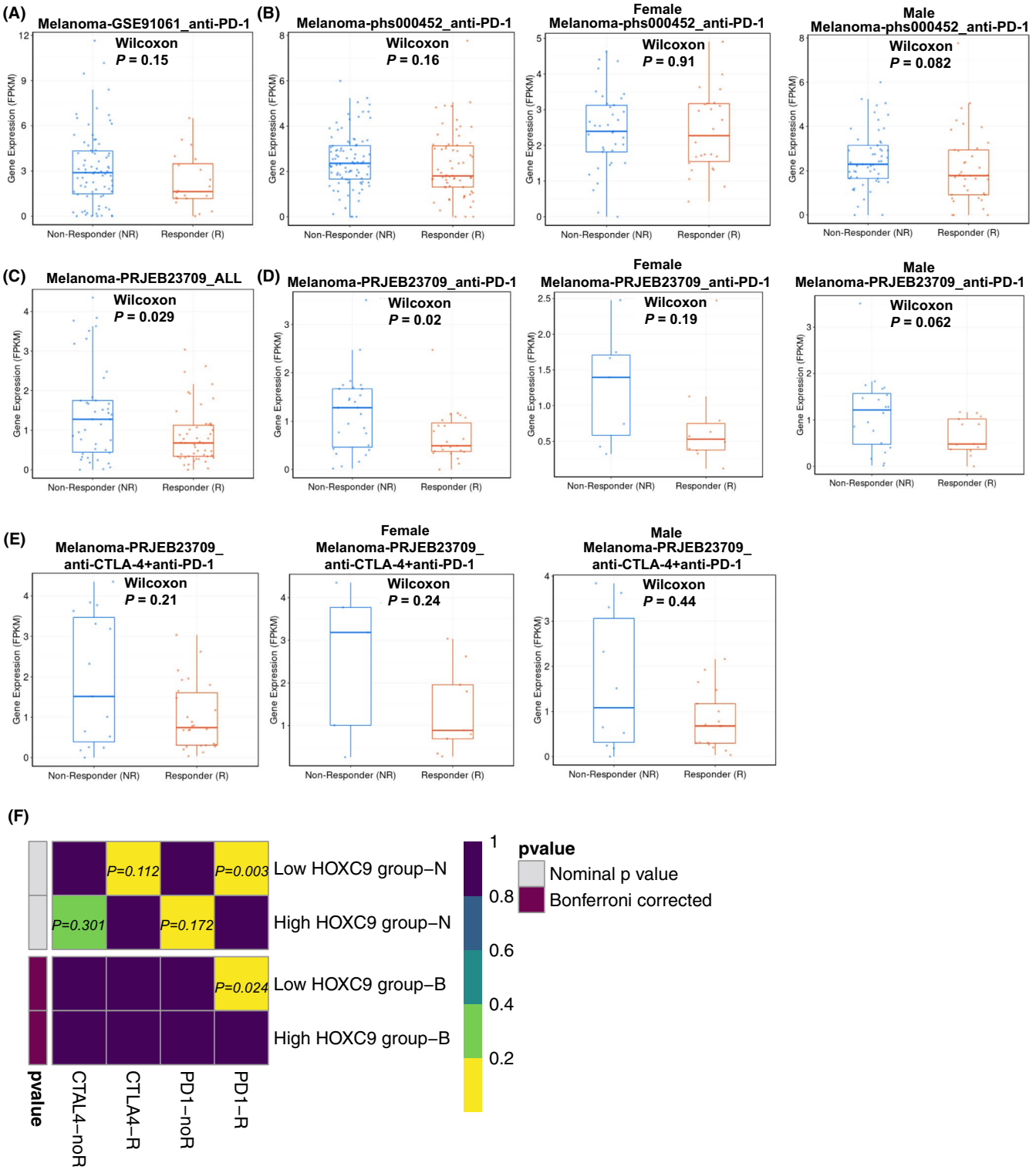

FIGURE 7 Correlation between *HOXC9* expression and immunotherapeutic response. A, TIGER database (http://tiger.canceromics.org/#/home) showed *HOXC9* expression between responders (R) and nonresponders (NR) in the anti-programmed cell death-1 (PD-1) GSE91061 cohort. B, TIGER database showed *HOXC9* expression between R and NR in the anti-PD-1 phs00452 cohort. C, TIGER database showed *HOXC9* expression between R and NR for all treatment in the PRJEB23709 cohort. D, TIGER database showed *HOXC9* expression between R and NR for anti-PD-1 in the PRJEB23709 cohort. E, TIGER database showed the *HOXC9* expression between R and NR for anti-CTLA4+anti-PD-1 in the PRJEB23709 cohort. F, SubMap analysis of the *HOXC9*-high and -low expression groups in The Cancer Genome Atlas gastric cancer cohort and four groups (anti-PD-1 responsive [-R] and nonresponsive [NR], and anti-CTLA-4-R and -NR) in a melanoma cohort treated with immune checkpoint inhibitors

an enhanced resistance to apoptosis by IFNγ signaling. Additionally, the *DAPK1* downstream tumor suppressor gene *RIG1* was downregulated, causing IFNγ resistance in GC treatment.

In conclusion, we identified and verified that *HOXC9* played an oncogenic role by inhibiting immune response in the GC immune microenvironment. Mechanistically, *HOXC9* exerted IFNγ resistance by downregulating the *DAPK1/RIG1/p-STAT1* axis in GC. Downregulated expression of *HOXC9* might sensitize cells to IFNγ. Our findings showed that the molecular mechanism of *HOXC9* provided a novel immunotherapeutic biomarker for GC in the future.

ACKNOWLEDGMENT

This work was supported by a grant from the young and middle-aged scientific and technological talents support program of Shenyang City (No. RC200554 to Chunli Wu).

CONFLICT OF INTEREST

None declared.

ORCID

Chunli Wu https://orcid.org/0000-0003-1809-6752

REFERENCES

1. Bray F, Ferlay J, Soerjomataram I, Siegel RL, Torre LA, Jemal A. Global cancer statistics 2018: GLOBOCAN estimates of incidence and mortality worldwide for 36 cancers in 185 countries. *CA Cancer J Clin*. 2018;68:394-424.
2. Plummer M, Franceschi S, Vignat J, Forman D, de Martel C. Global burden of gastric cancer attributable to *Helicobacter pylori*. *Int J Cancer*. 2015;136:487-490.
3. Thomassen I, van Gestel YR, van Ramshorst B, et al. Peritoneal carcinomatosis of gastric origin: a population-based study on incidence, survival and risk factors. *Int J Cancer*. 2014;134:622-628.
4. Chen PF, Wang F, Nie JY, et al. Co-expression network analysis identified CDH11 in association with progression and prognosis in gastric cancer. *OncoTargets and therapy*. 2018;11:6425-6436.
5. Comprehensive molecular characterization of gastric adenocarcinoma. *Nature*. 2014;513:202-209.
6. Li Z, Liu Z, Shao Z, et al. Identifying multiple collagen gene family members as potential gastric cancer biomarkers using integrated bioinformatics analysis. *PeerJ*. 2020;8:e9123.
7. Yang B, Zhang M, Luo T. Identification of potential core genes associated with the progression of stomach adenocarcinoma using bioinformatic analysis. *Front Genet*. 2020;11:517362.
8. Parker BS, Rautela J, Hertzog PJ. Antitumour actions of interferons: implications for cancer therapy. *Nat Rev Cancer*. 2016;16:131-144.
9. Platanias LC. Mechanisms of type-I- and type-II-interferon-mediated signalling. *Nat Rev Immunol*. 2005;5:375-386.
10. D'Errico M, de Rinaldis E, Blasi MF, et al. Genome-wide expression profile of sporadic gastric cancers with microsatellite instability. *Eur J Cancer*. 2009;45(3):461-469.
11. Oh SC, Sohn BH, Cheong JH, et al. Clinical and genomic landscape of gastric cancer with a mesenchymal phenotype. *Nat Commun*. 2018;9:1777.
12. Lei Z, Tan IB, Das K, et al. Identification of molecular subtypes of gastric cancer with different responses to PI3-kinase inhibitors and 5-fluorouracil. *Gastroenterology*. 2013;145:554-565.
13. Diboun I, Wernisch L, Orengo CA, Koltzenburg M. Microarray analysis after RNA amplification can detect pronounced differences in gene expression using limma. *BMC Genom*. 2006;7:252.
14. Horvath S, Dong J. Geometric interpretation of gene coexpression network analysis. *PLoS Comput Biol*. 2008;4:e1000117.
15. Wang H, Qiu P, Zhu S, et al. SET nuclear proto-oncogene gene expression is associated with microsatellite instability in human colorectal cancer identified by co-expression analysis. *Dig Liver Dis*. 2020;52:339-346.
16. Wang H, Zhang M, Zhang M, Wang F, Liu J, Zhao Q. Carboxypeptidase A6 was identified and validated as a novel potential biomarker for predicting the occurrence of active ulcerative colitis. *J Cell Mol Med*. 2020;24:8803-8813.
17. Wang HZ, Wang F, Chen PF, et al. Coexpression network analysis identified that plakophilin 1 is associated with the metastasis in human melanoma. *Biomed Pharmacother*. 2019;111:1234-1242.
18. Barbie DA, Tamayo P, Boehm JS, et al. Systematic RNA interference reveals that oncogenic KRAS-driven cancers require TBK1. *Nature*. 2009;462:108-112.
19. Hänzelmann S, Castelo R, Guinney J. GSVA: gene set variation analysis for microarray and RNA-seq data. *BMC Bioinformatics*. 2013;14:7.
20. Charoentong P, Finotello F, Angelova M, et al. Pan-cancer immunogenomic analyses reveal genotype-immunophenotype relationships and predictors of response to checkpoint blockade. *Cell Rep*. 2017;18:248-262.
21. Yoshihara K, Shahmoradgoli M, Martínez E, et al. Inferring tumour purity and stromal and immune cell admixture from expression data. *Nat Commun*. 2013;4:2612.
22. Koch A, De Meyer T, Jeschke J, Van Criekinge W. MEXPRESS: visualizing expression, DNA methylation and clinical TCGA data. *BMC Genom*. 2015;16:636.
23. Hoshida Y, Brunet JP, Tamayo P, Golub TR, Mesirov JP. Subclass mapping: identifying common subtypes in independent disease data sets. *PLoS One*. 2007;2:e1195.
24. Roh W, Chen PL, Reuben A, et al. Integrated molecular analysis of tumor biopsies on sequential CTLA-4 and PD-1 blockade reveals markers of response and resistance. *Sci Transl Med*. 2017;9(379):eaah3560.
25. Goubau D, Deddouche S, Reis e Sousa C. Cytosolic sensing of viruses. *Immunity*. 2013;38:855-869.
26. Takeuchi O, Akira S. Innate immunity to virus infection. *Immunol Rev*. 2009;227:75-86.
27. Beachboard DC, Horner SM. Innate immune evasion strategies of DNA and RNA viruses. *Curr Opin Microbiol*. 2016;32:113-119.
28. Hou J, Zhou Y, Zheng Y, et al. Hepatic RIG-I predicts survival and interferon-α therapeutic response in hepatocellular carcinoma. *Cancer Cell*. 2014;25:49-63.
29. Desta IT, Porter KA, Xia B, Kozakov D, Vajda S. Performance and its limits in rigid body protein-protein docking. *Structure*. 2020;28:1071-1081.e1073.
30. Zhao XF, Yang YS, Park YK. HOXC9 overexpression is associated with gastric cancer progression and a prognostic marker for poor survival in gastric cancer patients. *Int J Clin Oncol*. 2020;25:2044-2054.
31. Hu M, Ou-Yang W, Jing D, Chen R. Clinical prognostic significance of HOXC9 expression in patients with colorectal cancer. *Clinical laboratory*. 2019;65.
32. Hur H, Lee JY, Yang S, Kim JM, Park AE, Kim MH. HOXC9 induces phenotypic switching between proliferation and invasion in breast cancer cells. *J Cancer*. 2016;7:768-773.
33. Xuan F, Huang M, Liu W, Ding H, Yang L, Cui H. Homeobox C9 suppresses Beclin1-mediated autophagy in glioblastoma by directly inhibiting the transcription of death-associated protein kinase 1. *Neuro Oncol*. 2016;18:819-829.
34. Peng X, Kang Q, Wan R, Wang Z. miR-26a/HOXC9 dysregulation promotes metastasis and stem cell-like phenotype of gastric cancer. *Cell Physiol Biochem*. 2018;49:1659-1676.

35. Pai P, Sukumar S. HOX genes and the NF-κB pathway: a convergence of developmental biology, inflammation and cancer biology. *Biochim Biophys Acta*. 2020;1874:188450.
36. Hayashida T, Takahashi F, Chiba N, et al. HOXB9, a gene overexpressed in breast cancer, promotes tumorigenicity and lung metastasis. *Proc Natl Acad Sci USA*. 2010;107:1100-1105.
37. Irazoqui JE, Ng A, Xavier RJ, Ausubel FM. Role for beta-catenin and HOX transcription factors in Caenorhabditis elegans and mammalian host epithelial-pathogen interactions. *Proc Natl Acad Sci USA*. 2008;105:17469-17474.
38. Demaria O, Cornen S, Daëron M, Morel Y, Medzhitov R, Vivier E. Harnessing innate immunity in cancer therapy. *Nature*. 2019;574:45-56.
39. Antonia SJ, Vansteenkiste JF, Moon E. Immunotherapy: beyond anti-PD-1 and anti-PD-L1 therapies. *Am Soc Clin Oncol Educ Book*. 2016;35:e450-458.
40. Smyth EC, Nilsson M, Grabsch HI, van Grieken NC, Lordick F. Gastric cancer. *Lancet*. 2020;396:635-648.
41. Akin Telli T, Bregni G, Camera S, Deleporte A, Hendlisz A, Sclafani F. PD-1 and PD-L1 inhibitors in oesophago-gastric cancers. *Cancer Lett*. 2020;469:142-150.
42. Coutzac C, Pernot S, Chaput N, Zaanan A. Immunotherapy in advanced gastric cancer, is it the future? *Crit Rev Oncol Hematol*. 2019;133:25-32.
43. Lordick F, Shitara K, Janjigian YY. New agents on the horizon in gastric cancer. *Ann Oncol*. 2017;28:1767-1775.
44. Zayac A, Almhanna K. Esophageal, gastric cancer and immunotherapy: small steps in the right direction? *Transl Gastroenterol Hepatol*. 2020;5:9.
45. Ivashkiv LB. IFNγ: signalling, epigenetics and roles in immunity, metabolism, disease and cancer immunotherapy. *Nat Rev Immunol*. 2018;18:545-558.
46. Ni L, Lu J. Interferon gamma in cancer immunotherapy. *Cancer Med*. 2018;7:4509-4516.
47. Ayers M, Lunceford J, Nebozhyn M, et al. IFN-γ-related mRNA profile predicts clinical response to PD-1 blockade. *J Clin Investig*. 2017;127:2930-2940.
48. Yang S, Wei J, Cui YH, et al. m(6)A mRNA demethylase FTO regulates melanoma tumorigenicity and response to anti-PD-1 blockade. *Nat Commun*. 2019;10:2782.
49. Dosset M, Vargas TR, Lagrange A, et al. PD-1/PD-L1 pathway: an adaptive immune resistance mechanism to immunogenic chemotherapy in colorectal cancer. *Oncoimmunology*. 2018;7:e1433981.

SUPPORTING INFORMATION

Additional supporting information may be found online in the Supporting Information section.

How to cite this article: Tang Y, Wang T, Yu Y, Yan Y, Wu C. Upregulation of *HOXC9* generates interferon-gamma resistance in gastric cancer by inhibiting the DAPK1/RIG1/STAT1 axis. *Cancer Sci*. 2021;112:3455–3468. https://doi.org/10.1111/cas.15043